ISOSPIN AND CLUSTERING AT MID-RAPIDITY IN INTERMEDIATE ENERGY HEAVY-ION REACTIONS*

L.G. Sobotka

Department of Chemistry, Washington University
St. Louis MO 63130, USA

(Received April 4, 2000)

The n/p asymmetry of the material found in the mid-velocity or "neck" region of an intermediate energy heavy-ion reaction is determined. In order to accomplish this task data from two different experiments are utilized. While the n/p asymmetry of the light particles is enriched in neutrons relative to the bulk matter, the total material found at mid-rapidity has an asymmetry very little different from that of the bulk system. This implies that, for the reaction studied, isospin equilibration plays a minor role in determining the isospin of the material found in the intermediate velocity region.

PACS numbers: 25.70.Lm, 25.70.Mn, 25.70.Pq

1. Introduction

Previous work by us [1, 2] and the INDRA collaboration [3] indicates that light charged-particles emitted in the intermediate-velocity region of peripheral to mid-central heavy-ion collisions are neutron-rich relative to those fragments emitted by the projectile and target-like fragments. This apparent neutron enrichment in the central region might be due to one or more of the following.

1. The influence of clustering, which can have the effect of amplifying a slight overall neutron enrichment of a system when one examines only the light ejectiles.

2. A natural consequence of a Coulomb suppression of the more highly charged species in sequential decay.

* Presented at the Kazimierz Grotowski 70$^{\rm th}$ Birthday Symposium "Phases of Nuclear Matter", Kraków, Poland, January 27–28, 2000.

3. The influx of neutrons into the emerging region between the re-separating projectile and target-like fragments.

The third potential explanation is the most interesting in that such a process can be understood as an equilibrium isospin fractionation effect between regions of different density. As a result of the fractionation, the material at mid-velocity would have a different overall n/p ratio than the value for the overall system. This equilibration process would tend to increase the neutron excess of the low density (surface-like) "neck" region at the expense of the material in the projectile and target velocity regions. We have done both model calculations and experimentation aimed at determining whether such a process occurs. The calculations serve as a guide to help us define the relevant physics while the experiments must answer the question of whether the total mid-velocity material has the same n/p ratio as the overall system. These calculations as well as the data will be presented in this talk.

2. Some relevant calculations

The physics relevant to the interesting potential reaction scenario is that at equilibrium, the chemical potentials of neutrons and protons (μ_n and μ_p) must be unique even if the system has regions of vastly different density. To satisfy this requirement, the partition of neutrons and protons between regions of different density need not be, and in general is not, uniform. This isospin partition upon phase separation has been discussed by both Barranco and Buchler [4] and Glendenning [5]. More recently this issue has been analyzed, within a relativistic mean field model for nuclear matter, by Müller and Serot [6]. Two figures from the latter reference are reproduced below.

The phase coexistence region is shown in Figure 1(a). Not only does the critical temperature depend on the proton fraction y, but the low density (gas) and the high density (liquid) can have substantially different n/p ratios. This is illustrated most clearly on the right hand side of this figure where the isothermal slice at $T = 10$ MeV through the coexistence region is shown. The composition of the vapor (left boundary of the coexistence region) is neutron rich relative to the liquid region (right boundary). The exception to this statement is the special n/p mix which can be taken through the phase transition without fractionation. This composition (the azeotrope) just so happens to satisfy both Gibbs conditions ($\mu_n^l = \mu_n^v$ and $\mu_p^l = \mu_p^v$) with an equal partitioning of n's and p's. Not surprisingly the azeotrope occurs at symmetry for (uncharged) nuclear matter. Dempsey [7] investigated the influence of charge. He found that the azeotropic composition shifts toward β-stability and that the magnitude of the fractionation is somewhat reduced when Coulomb effects are considered. The reason that the sense of the

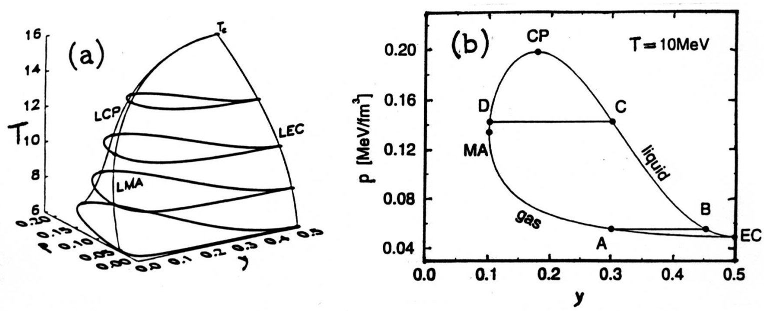

Fig. 1. The phase coexistence region of nuclear matter shown as a function of temperature, pressure and proton fraction (T, P, y) (a) and the isothermal slice (T=10 MeV) from the dinodal region (b) from the calculations of Ref. [6]. At hydrostatic equilibrium the vapor composition (left boundary of coexistence region) is enriched in neutrons relative to the liquid phase (right boundary of the coexistence region.) The quantity of each phase is determined by the standard "tie-line" rule of the Maxwell construction.

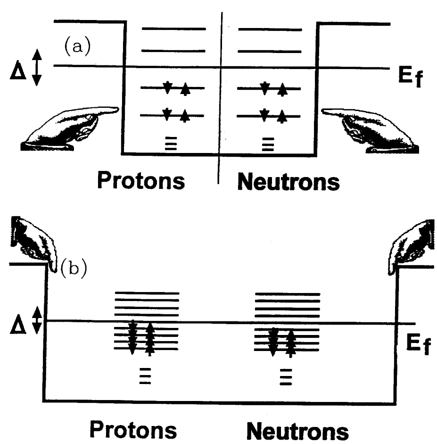

Fig. 2. A cartoon of the physics which motivates this work

fractionation is the same in charged finite systems as in nuclear matter is that the Coulomb energy depends more weakly upon the density ($\rho^{1/3}$) than does the symmetry energy (kinetic portion $\propto \rho^{2/3}$).

Before moving on it is worthwhile to illustrate this physics with a cartoon. The kinetic portion of the symmetry energy is proportional to the level spacing at the Fermi surface (Δ) which in turn depends on the system density (ρ). You can imagine the system to be the overlap region in a heavy-ion collision and the fingers pulling the system towards low density to be the receding target-like and projectile-like fragments. *If* this central part of the system remains in isospin equilibrium with the saturated target-like and projectile-like fragments while the density of the central region is reduced below saturation, one expects a neutron inflow and a proton outflow from this central region as long as the bulk system is neutron rich relative to the azeotrope. In other words: as long as there is sufficient time and n-excess, and new extended surface regions are being created, one expects the new low density regions to become neutron rich.

In passing (and in response to a question from the organizer of this conference) it is worth asking if there can be a measurable neutron enrichment (as compared to the bulk) at mid-velocity in a peripheral HI reaction simply by virtue of a pre-existing n-skin? The answer is "no" as long as there are more than about a dozen nucleons in the overlap region. This is illustrated in Fig. 3 which makes use of the Thomas–Fermi Model of Myers and Swiątecki [8]. Sections (a), (b) and (c) show the density profiles, n/p ratio and the number of nucleons external to a given radius as calculated by this model for ^{136}Xe. Sections (d) and (e) of this figure show the n/p ratio and the number of nucleons in the overlap region swept out when two such nuclei collide. The overlap region has essentially the bulk composition with the exception of the very most peripheral collisions for which the size of the overlap region is reduced to less than a dozen nucleons. Examination of the charge profiles from electron scattering suggests that even this modest effect is overestimated by this Thomas–Fermi calculation. (I should also point out that increasing the overall n-excess, say to ^{142}Xe, makes only a modest change to the number of nucleons in the overlap region with N/Z significantly greater than that of the bulk system.)

Before turning to the experimental data, I want to present some BUU calculations which shed some light on the dynamical issues associated with isospin equilibration between regions of different density and on the possible influence of clusterization on experimental observables.

The calculations [9] presented in Fig. 4 use the formulation of Danielewicz and Bertsch for creating, transporting and destroying d, t, and ^{3}He clusters [10]. These calculations show the total density profile ((a),(b),(c)) and that for the *free* n's ((d),(e),(f)) and p's ((g),(h),(i)) at three different times ($t = 0$, 50, and 100 fm/c). The final time step shows an excess of free neutrons relative to protons in the "neck" region. The question is — with these calculations as it will be with the data — is there really an excess of n's at mid-velocity? This question is answered (for this calculation) in the three frames on the right hand side ((j),(k),(l)). Here the total (open symbols) and free (closed symbols) n/p ratios are presented as a function of the distance from the projection of the coordinate position onto the separation axis to the system center of mass (D). Overall, the center of the neck region ($D = 0$) is only slightly enriched in neutrons (reflecting some isospin equilibration) but

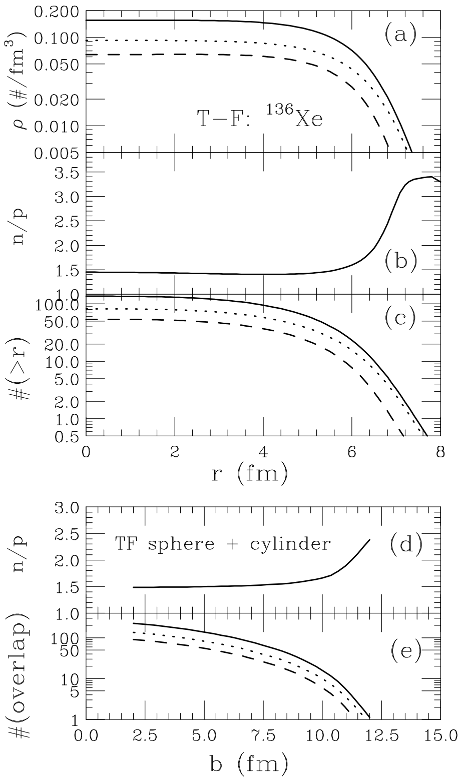

Fig. 3. Density profiles (a) n/p ratio (b) and nucleons external to the given radius (c) for ^{136}Xe as calculated from a Thomas–Fermi model. Sections (d) and (e) show the n/p ratio and the number of nucleons in the overlap region, as a function of impact parameter when two nuclei of this type collide. In these plots the total, proton and neutron distributions are given by solid, dashed and dotted lines, respectively.

the free neutrons far exceed the free protons. The difference is due to the fact the central region is highly clustered with an overall symmetric participation in the clustering. In other words, the effect of clustering (on the free n/p ratio) is to amplify the modest overall n-excess.

We remind the reader that experimentally all that had been observed prior to the work described below is that certain isotopic and isobaric ratios (such as $t/^3$He) are much larger at mid-velocity than in the projectile velocity region [1–3,7]. Our recent experimental effort sought to answer the question of whether in fact the total n/p ratio of the mid-velocity region is different than that of that of the bulk system.

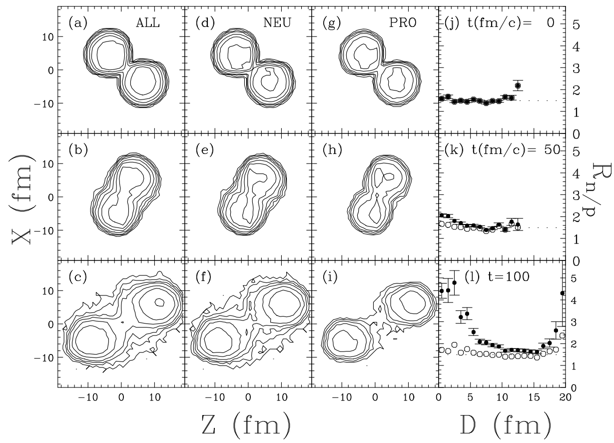

Fig. 4. Boltzmann–Uehling–Uhlenbeck simulation of a collision between ^{136}Xe and ^{124}Sn at 55 MeV A and an impact parameter of 8.8 fm. The different panels show projections (in the plane defined by the projectile momentum and the impact parameter) of the total ((a),(b),(c)), neutron ((d),(e),(f)) and proton ((g),(h),(i)) densities. The nucleons bound in light clusters are excluded from the contour plots ((d)–(i)). Sections ((j)–(l)) display the neutron-to-proton ratio $R_{n/p}$ as a function of the magnitude D of the projection of the space coordinates on the projectile-target separation axis, excluding (solid) and including (open) the nucleons bound in small clusters. $D = 0$ corresponds to the center of mass position.)

3. Data (old and new)

To date charged-particle data has been presented for a number of systems at several energies. By far the most complete and comprehensive data have been collected by the INDRA collaboration for the ^{129}Xe+$^{\rm nat}$Sn system between 25–50 MeV/A [3,11]. This work decomposes the charged-particle yield into components arising from 1) evaporation from the target and projectile-like sources and 2) a mid-velocity source. What is missing from this work is data on the free neutrons and isotopic information in the Intermediate-Mass Fragments (IMF$'s$). In a recent experiment by our group we sought to fill these gaps. We studied ^{129}Xe+^{120}Sn collisions at $E/A = 40$ MeV. The INDRA data set includes a study at 39 MeV/A. There is no reason to believe the slight difference in energy or the isotope mix (in the INDRA target) are differences of consequence. However the difficulty of splicing together these two sets is non-trivial due to the demands on experiments designed to collect quality (free) n data.

Acquiring data on neutron emission patterns, which allows for a source decomposition analysis, requires excess scattering material be kept to a minimum. Therefore such data cannot be collected in the same experiment as one which characterizes the charged-particle emission patterns with a 4π detector. As a result, standard impact parameter selectors (which make use of 4π counting) cannot be used. However as we desire to compare to the peripheral to mid-central data from INDRA, some impact parameter selection must be provided. In order to accomplish this we have measured both the charge of the projectile-like fragment ($Z_{\rm PLF}$) and α-particle spectra. (As you will see some limited data were also collected for the IMF's). Previous work [2] indicates that the charge of the projectile-like fragment $Z_{\rm PLF}$ is inversely related to the average charged-particle multiplicity and thus can be used as a measure of centrality. In the present work we select projectile-like fragments emitted to angles just beyond the grazing angle with charge $15 < Z_{\rm PLF} < 35$. This gate eliminates the most central collisions, for which no large projectile remnant remains, and the most peripheral collisions for which only modest evaporation from the projectile-like fragment has occurred. However such a selection is rather crude and we have, a priori, no knowledge of the actual impact parameter window selected. On the other hand, the α-particle data can be compared to those collected with 4π detectors to provide a fix on the impact parameter region selected.

Projectile-like fragments (PLFs) were detected between 4.6° to 9.3° in an annular Si–CsI(Tl). This telescope provided the atomic number and energy of the PLF's. Four charged-particle telescopes, consisting of two Si layers backed by CsI(Tl), were used to detect α-particles. The Si layers are part of the LASSA array [12] and consist of 16-strip dE (65 μm) and orthogonally oriented 16-strip E (1000 μm) detectors, both of which are 50 $\times$ 50 mm. Four 2-cm thick CsI(Tl) detectors were positioned, in a quadrant arrangement, behind the Si strip detectors. This thickness is sufficient to stop all of the α-particles but insufficient for the hydrogen isotopes. The telescopes were run at two sets of angles. For analysis purposes, angles were defined by the CsI(Tl) positions, two angles per telescope. Thus this data set contains data for 16 different polar angles. These telescopes were calibrated with α-particle and deuteron elastic scattering at small angles. The charged-particle detectors, along with two CsF scintillators (see below) were positioned inside of a thin walled (3.2 mm) Al scattering chamber of 80 cm diameter.

Neutrons were detected in a set of 15 discrete BC501A scintillators with cylindrical volumes, 7.6 cm thick and 11.4 cm in diameter. These detectors varied in distance from the target from 2200 to 1200 mm for forward to backward angles, respectively. The n-detectors where used in conjunction with plastic paddles positioned in front of the n-detectors and the two small (20 mm $\times$ 40 mm) CsF detectors positioned close to the target. The former were used to veto charged particles which penetrated the vacuum vessel and the latter provided the start for the time-of-flight measurement. The overall (all pulse heights) time resolution as determined from the γ-ray flash was 2.1 ns (FWHM). The efficiencies of the n-detectors were calculated with the code SCINFUL [13]. The low-energy efficiency was verified via a calibration with ^{252}Cf [14]. The thresholds were set in software to be 200 keeV. Interference from the subsequent beam burst coupled with the long flight distance (at forward angles) limited our ability to study the emission of very low energy neutrons.

Charged-particle invariant cross section maps have been published for several intermediate-energy systems including the one studied here [3]. Fig. 5 provides the neutron invariant cross section map for the system and event selection of the present work. Due to the absence of Coulomb rings, the source patterns are not apparent. Nevertheless, source fits clearly indicate the need for multiple sources. A three moving source parameterization was used to fit both the α-particle and neutron data. In the fit to the α-particle data, all the multiplicities and temperatures were allowed to vary. The velocities of the projectile-like and target-like sources were also allowed to vary. The mid-velocity source was fixed at the center-of-mass velocity and the Coulomb barriers were fixed at 8 MeV for the target and projectile sources. A Gaussian variation of the Coulomb barriers of 50% was also included. The projectile and target-like sources were taken to be of the surface type while a volume type was used for the mid-velocity source. This fitting procedure is similar to that used previously for fitting charged-particle data from intermediate-energy heavy-ion reactions [15]. In fitting the neutron data, the projectile and target-like source velocities were fixed at the values extracted from the fits to the α-particle data (see below). In this case, the fits were done using relativistic Maxwell–Boltzmann distributions folded with a

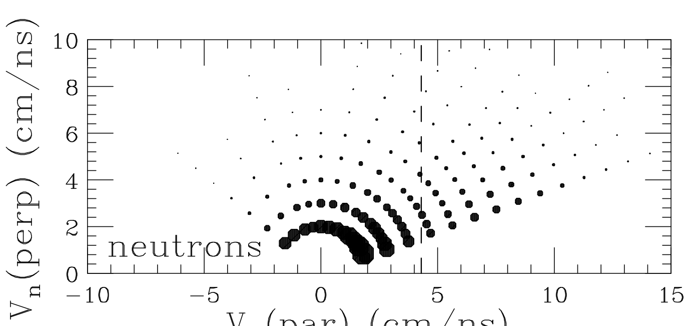

Fig. 5. Invariant neutron cross section plot for the system $E/A=$ 40 MeV ^{129}Xe $+^{120}$Sn when PLF's are detected just beyond the grazing angle with $15 < Z_{\rm PLF} < 35$. The area of the plotted symbols is proportional to the cross section. The dashed line indicates the center of mass velocity.

resolution function (derived from a Gaussian distribution in time.) The significance of relativity is much less than that of the finite velocity resolution. The fits to the α-particle data, shown in Fig. 6, represent the data very well while those for the n-data, Fig. 7, suggest the need for additional forward and backward components, each with small multiplicity.

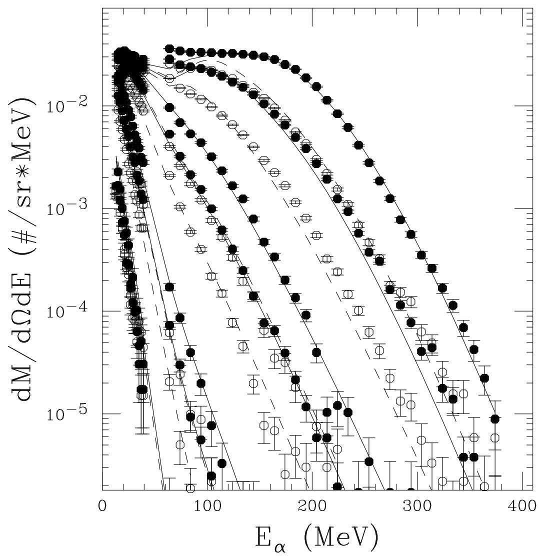

Fig. 6. α-particle data from selected angles and fits using a three source model

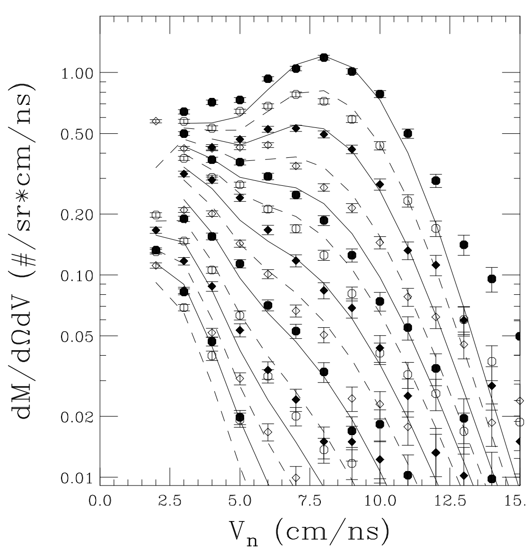

Fig. 7. Neutron data and fits using a three source model

The extracted multiplicities from the mid-velocity source (MID) and the sum of the target-like and projectile-like sources (T+P) are shown in Fig. 8 as the "bird-like" symbols. The charged-particle data from INDRA are also shown for the 4 most peripheral bins reported by Plagnol *et al.* [11]. These charged-particle data span from $b = 10$ fm to $b = 4$ fm, (bins 1 through 4 respectively, see [11].) Each element is presented as a different symbol and we have dispersed the data from the four bins by addition of abscissa offsets which increase with increasing centrality (see figure caption.) First we should focus on the α-particle data. Our data, in terms of both the (a) mid-velocity and (b) target + projectile multiplicities (and thus the ratio (c) are very close to those extracted from the INDRA data for bins 3 and 4. These bins correspond to the impact parameter window $4 < b < 7$. This

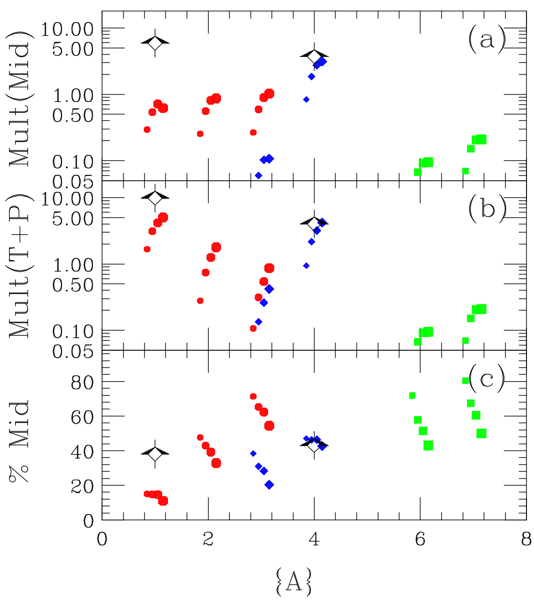

Fig. 8. The multiplicities of neutrons and charged particles from the mid-velocity (a) and target and projectile-like sources (b) as well as the mid-velocity fraction (c), are shown for $E/A = 40$ MeV Xe+Sn. The neutron and alpha data from the present experiment are shown as the "bird-like" symbols. The charged particle results from the four most peripheral bins from the INDRA study of the same system are also displayed. In order to display all 4 bins, the data are dispersed about the actual atomic mass number left to right (smaller to larger symbols) with increasing centrality. These 4 bins (1–4) correspond to deduced impact parameter selections of: $10 > b > 8.5$, $8.5 > b > 7.0$, $7.0 > b > 5.5$, and $5.5 > b > 4.0$ (see [3].) The $Z = 1, 2$ and 3 data are shown as circles, diamonds and squares respectively.

window is consistent with our expectation that the PLF selection removed both the most central and peripheral events. Some additional confidence that the data sets can be compared comes from the extracted velocities of the quasi-projectiles. The fits to the α-particle data, for which the projectile and target velocities are free parameters, gave projectile (target) velocities of $\beta_{\rm cm} = 0.107$ (-0.103), values close to those extracted from the 4π charged-particle data ($\beta_{\rm cm}^{\rm PLF} = 0.120$ and 0.111 for bins 3 and 4, respectively [16].)

For this event selection, the neutron multiplicity is almost 10 times the proton multiplicity at mid-velocity while only a factor of about 2 times more for the projectile-like and target-like velocity regions. While the fraction of neutrons emitted in the mid-velocity region (see Fig. 8(c)) is substantially greater than that for protons, it is about equal to that for deuterons and α-particles. Other trends which can be seen from this figure are the marked tendency for the heavier hydrogen isotopes and heavy clusters to be found at mid-velocity. While these trends have been previously noted, another observation can be made from this plot which would surprise many. There is a clear decrease in the relative emission of the rare particles at mid-velocity with increasing centrality. While the magnitude of this trend may be influenced by the extraction procedure, it suggests that the emission mechanisms and/or the relative position on excitation functions, increasingly favors rare particle emission from the target and projectile-like sources as the centrality increases.

The presentation of these data in terms of the fractional (mid-velocity) yield also highlights an important feature which is best illustrated by the $t/^3$He (circles/diamonds at $A \sim 3$) comparison. One expects that ^{3}He emission will be suppressed (relative to t emission) more for highly charged sources and that this bias will diminish as the temperature increases. Experimentally one finds that the $t/^3$He ratio is larger for the higher temperature mid-velocity source than it is for the sources associated with the projectile and target-like sources. This indicates that the influence of the kinetic Coulomb factors are still quite strong for these reactions.

While the INDRA data provide an estimate of the IMF multiplicity, the isotope composition was not determined for these fragments. The LASSA detectors however do provide this information up to $Z = 6$, albeit (in this experiment) in a fashion which does not allow for a source decomposition. Figure 9 shows an example of a particle identification (PID) spectrum at a laboratory angle of 25°. Assuming that the IMF's detected at this angle are representative of those from the mid-velocity source [18], we find that the mean values of (N/Z) are 1.18, 1.02, 1.32, 1.26, 1.23 and 1.13 for $Z = 1, 2, 3, 4, 5$ and 6, respectively.

The measured multiplicities and the measured values of (N/Z) allow us to estimate the composition of the material found at mid-velocity as well as

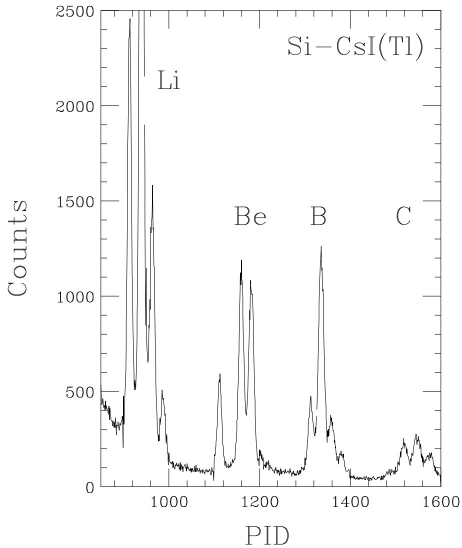

Fig. 9. Example PID spectrum. This is from a detector at $\Theta_{\mathrm{lab}} = 25°$and uses the Si-CsI(Tl) pulse heights. The C data are underrepresented in this plot as many of these fragments are stopped in the second Si telescope element.

determine the overall charge partition of the selected reactions. The particle tally is presented in Table I. The bulk of the charge resides in the projectile-like (detected) and target-like (inferred) residues. The mean value of the PLF charge is 25 and due to fact that the system is nearly symmetric the mean value of Z_{tlf} must be similar. Thus about 1/2 of the total system charge resides in these fragments. Of the remainder, about $3/5^{\mathrm{ths}}$ (∼30 units) is evaporated from the target and projectile-like fragments and $2/5^{\mathrm{ths}}$ (∼20 units) comprise the mid-velocity source. Using the measured multiplicities

TABLE I

Particle Tally

	n	H	He	IMF	heaviest	total
M_{mid}	5.5	2.6	3.5	2.0	–	13.6
Z_{mid}	0	2.6	7.0	∼10	–	**20**
A_{mid}	5.5	5.7	14.1	22		47
$(N/Z)_{\mathrm{mid}}$	–	1.18	1.02	∼ 1.2	–	**1.4**
M_{TP}	11.3	7.7	4.7	2.	2	28
Z_{TP}	0	7.7	9.4	∼ 10	∼ 50	**77**
$(N/Z)_{\mathrm{TP}}$	–	0.458	0.97	–	–	–

for the isotopically resolved light ions, the measured IMF multiplicity (from INDRA) and mean IMF N/Z ratio (our experiment for $Z \leq 6$) we find that the mid-velocity source is of modest mean size (~47 nucleons) with $(N/Z)_{\rm mid} \sim 1.4$. The latter value is indistinguishable from that of the bulk system $(N/Z)_{\rm sys} = 1.394$. On the other hand a value of $(N/Z) = 1.4$ is neutron rich relative to β-stability for a system of the size of the mid-velocity source. I would like to mention that if one does not include the IMF's in the particle tally, the extracted value of $(N/Z)_{\rm mid}$ would be significantly greater than the value for the bulk system.

An understanding of this intermediate-velocity zone clearly requires a dynamical model which treats clusters. Nevertheless a schematic equilibrium model can provide considerable insight. Figure 10 presents the results of a preliminary micro-canonical calculation. This calculation considers all partitions of 46 nucleons, 27 neutrons and 19 protons, into fragments with $Z \leq 4$ and $A \leq 10$. Many excited states, both bound and unbound, are explicitly considered. To account for the heavier IMF's, not explicitly considered, a pseudo heavy IMF is included with the correct value of (N/Z) and a degeneracy adjusted to reproduce the experimental multiplicity of fragments with $Z > 4$. This calculation makes use of the techniques described by Randrup [17] to evaluate the phase space integrals for each possible configuration, all of which are included in an enumeration. The reason we have taken this exact enumeration procedure is that it readily allows us to explicitly consider excluded volume effects. Specifically we exclude volumes consistent with wave function sizes (see figure caption.) The expected multiplicities (top sections) and two interesting ratios (bottom sections) are shown for 3 different densities. What is most striking about this calculation is that the deuteron yield (dashed line) is extremely sensitive to the system volume. At high density (a) the deuteron yield is substantially below that of tritons over the entire energy range. The depletion of deuterons is due to both the small binding energy and large intrinsic volume of these particles. When the volume is increased to that of a sphere of 8 fm (section c) the large size of the deuteron is of little consequence and the yield increases. This illustrates how the large size of the deuteron make it an extremely sensitive indicator of the system volume, an indicator which has not been utilized before. The experimental data are shown as solid symbols (b) at a value of the energy per nucleon for which there is a favorable comparison between the data and calculations. At this low energy ($E/A \sim 5$ MeV) about 75% of the matter is in well bound fragments, the hydrogen isotopes all have about the same yield, and the yield of ^{3}He is lower than that of the t's by about a factor of 10. These simple calculations indicate that the observed large mass fraction in well bound particles, the large $t/^3$He ratios and significant d yields are the equilibrium expectation for a rather dilute, modestly excited

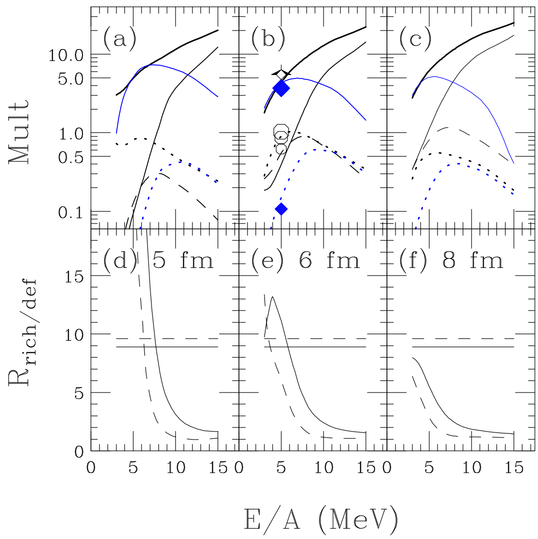

Fig. 10. Results of microcanonical calculations for 46 nucleons, 19 proton and 27 neutrons in volumes equal to that of spheres of radii 5 ((a),(d)), 6((b),(e)) and 8 fm ((c),(f)). Fragments with $Z \leq 4$ and $A \leq 10$ are explicitly considered in this calculation. In sections (a)–(c) n, p and α-particles are represented by solid lines, (d) by the dashed lines and t and ^{3}He by dotted lines. The neutron multiplicity is always the largest while α-particles (protons) are the second most prevalent at low (high) energies. The experimental data for $Z = 0$, 1 and 2 are displayed in section (b) as the bird-like, circle and diamond symbols, respectively. The larger the symbol the heavier the isotope. Sections (d)–(f) provide the free n/p and $t/^3$He ratios as solid and dashed lines. The experimental values are shown as horizontal lines. The excluded volumes for the light ions are calculated with the following radii: 0.8, 0.8, 2.2, 1.9, 1.9, 1.6 for $n, p, d, t,$ ^{3} He and α-particles, respectively. The excluded volumes of the heavier fragments use a radius parameter if 1.4 fm.

system. While the excitation energy per nucleon is consistent with the values of the fit temperatures for this source (~7 MeV), the nature of the data (broad impact parameter range) and the sensitivity of the calculations to the total and particle (excluded) volumes, suggest that precise determination of the best value of E/A is without merit.

In summary, our results suggest that the mid-velocity region is similar in N/Z to the bulk material. Preliminary calculations suggest that the light fragment composition is roughly what one would expect from an equilibrium partition of a system of the correct total nucleon and isospin composition if the partitioning occurs at low density with an energy per nucleon similar to but not exceeding the saturation value of the binding energy per nucleon.

I would like to thank Drs. E. Plagnol and A. Chbihi for providing the INDRA results in tabular form. I must also thank my collaborators in St. Louis, Drs. R.J. Charity and J.F. Dempsey. This work was supported by the U.S. Department of Energy under Grant No. DE-FG02-87ER40316.

REFERENCES

[1] J. Tõke, B. Lott, S.P. Baldwin, B.M. Quednau, W.U. Schröder, L.G. Sobotka, J. Barreto, R.J. Charity, D.G. Sarantites, D.W. Stracener, R.T. de Souza, *Phys. Rev. Lett.* **75**, 2920 (1995).

[2] J.F. Dempsey, R.J. Charity, L.G. Sobotka, G.J. Kunde, S. Gaff, C.K. Gelbke, T. Glasmacher, M.J. Huang, R.C. Lemmon, W.G. Lynch, L. Manduci, L. Martin, M.B. Tsang, D.K. Agnihotri, B. Djerroud, W.U. Schröder, W. Skulski, J. Tõke, W.A. Friedman, *Phys. Rev.* **C54**, 1710 (1996).

[3] Łukasik, *et al.*, (INDRA collaboration), *Phys. Rev.* **C55**, 1906 (1997).

[4] M. Barranco, J.R. Buchler, *Phys. Rev. C* **22**, 1729 (1980).

[5] N.K. Glendenning, *Phys. Rev.* **D46**, 1274 (1992).

[6] H. Müller, B.D. Serot, *Phys. Rev.* **C52**, 2072 (1995).

[7] J.F. Dempsey, PhD thesis, Washington University, Department of Chemsitry (1997).

[8] W.D. Myers, W.J. Swiatecki, *Nucl. Phys.* **A601**, 141 (1996).

[9] L.G. Sobotka, J.F. Dempsey, R.J. Charity, P. Danielewicz, *Phys. Rev.* **C55**, 2109 (1997).

[10] P. Danielewicz, G.F. Bertsch, *Nucl. Phys.* **A533**, 712 (1991); P. Danielewicz, *Phys. Rev.* **C51**, 716 (1995).

[11] E. Plagnol, *et al.*, INDRA collaboration, *Phys. Rev.* **C61**, 014606 (2000).

[12] B. Davin *et al.*, LASSA collaboration, report in preparation, Indiana University.

[13] Computer code SCINFUL, J.K. Dickens, ORNL-6462 (1988), NEA Data Bank Program: PSR-0267 (1994).

[14] C. Wagemans, *The Nuclear Fission Process*, CRC Press, Boca Raton, 1991, ch.11.

[15] D.J. Fields, *et al.*, *Phys. Rev.* **C34**, 536 (1986).

[16] Two methods were used in [11] to extract source parameters. The velocities given are for method (I), the method used to extracted the multiplicities for charged particles used in the present work.

[17] J. Randrup, *Comput. Phys. Commun.* **59**, 439 (1990).

[18] The invariant cross section maps of the IMF's [3], indicated that the IMF's from the projectile-like fragment are predominately located at even more forward angles.